Templated Crystallisation of Calcium and Strontium Carbonates on Centred Rectangular Self-Assembled Monolayer Substrates

Jörg Küther, Gabriele Nelles, Ram Seshadri, Matthias Schaub, Hans-Jürgen Butt, and Wolfgang Tremel*

Abstract: The calcite and vaterite modifications of $CaCO_3$ possess threefold symmetry axes in their crystal structures, while the aragonite modification does not. Since many self-assembled monolayers (SAMs) of simple thiols on gold organise in a hexagonal close-packed manner, patterns for the templated crystallisation of the first two polymorphs on SAMs are simple to achieve. This is not true in the case of aragonite. A substituted disulphide derived from anthracene-2-carboxylic acid, which has been previously established as forming centred rectangular lattices when assembled on a gold (111) surface, has therefore been employed to form substrates for the crystallisation of $CaCO_3$ with the specific intention of preferentially inducing the growth of aragonite. For comparison, we have also performed such crystallisations on a SAM substrate derived from hexadecane thiol. While the crystallisation of the $CaCO_3$ polymorphs is invariably accompanied by the problem of competing phases, $SrCO_3$ crystallises from solution uniquely in the strontianite modification, which is isostructural with aragonite. We have thus performed the crystallisation of $SrCO_3$ as well and present the results.

Keywords: alkyl thiol · aragonite · biomineralization · calcium · crystal growth

Introduction

There exists sustained interest in understanding natural biomineralisation processes[1] typified by the ability of small amounts of organic substances to determine the modes of crystallisation of certain inorganic materials. Central to these studies is the templated crystallisation of calcium carbonate in its three ubiquitous polymorphs, calcite, vaterite and aragonite, on substrates whose specific surface structure can be controlled. Such studies have included the crystallisation of calcium carbonate on surfaces modified with proteins,[2] beneath Langmuir monolayers at the air–water interface[3] and on self-assembled monolayers (SAMs) of alkylsilyl compounds on Si wafers.[4] Additionally, there has been some interest in growing crystals of the calcium carbonate polymorphs in polymers[5] and in bicontinuous emulsions;[6] these are of interest from a materials perspective rather than from the viewpoint of understanding natural biomineralisation processes. Our recent work in the area of templated crystallisation/model biomineralisation has focused on the use of SAMs of ω-substituted alkylthiols on Au (111) as substrates for templating the crystallisation of $CaCO_3$ in its different crystal modifications. We have been guided by the broad principles that the surface structure of the SAMs can be determined through atomic force microscopy (AFM) and can be correlated with the polymorphism and habits of the $CaCO_3$ crystals they template and, further, that the polarity of the surface layer can be controlled through changing the ω functionality.

Our previous contributions on this subject have been concerned less with microscopic detail than with some general aspects of $CaCO_3$ crystallisation on SAMs of substituted alkylthiols on gold.[7, 8] This has included establishing whether the substrate truly acts as a template, followed by studies on the effects that temperature, the nature of the ω substituent and the length of the alkyl chain of the thiol may have upon the relative and absolute amounts of the polymorphs of $CaCO_3$ formed on the SAMs. During these studies, we have observed that aragonite is usually formed only when crystallisation is carried out at 45 °C instead of 22 °C. Rietveld refinement of X-ray powder diffraction (XRD) profiles has proved to be a useful tool in estimating the relative amounts

[*] Prof. W. Tremel, J. Küther, Dr. R. Seshadri
Institut für Anorganische Chemie und Analytische Chemie
Johannes Gutenberg-Universität Mainz, Becherweg 24
D-55099 Mainz (Germany)
Fax: (+49) 6131-39-3922
E-mail: tremel@indigotrem1.chemie.uni-mainz.de
Dr. G. Nelles, Prof. H.-J. Butt
Institut für Physikalische Chemie
Johannes Gutenberg-Universität Mainz, Welderweg 11
D-55099 Mainz (Germany)
Dr. M. Schaub
W. C. Heraeus GmbH, Heraeusstr. 12–14, D-63450 Hanau (Germany)

0947-6539/98/0409-1834 $ 17.50+.50/0

(weight fractions) of the different polymorphs and thus proved crucial to obtaining a heuristic view of the processes taking place.

In this contribution we focus on two distinct substrates and their effect on templating the crystallisation of $CaCO_3$. The substrates are SAMs of mercapto hexadecane [$CH_3(CH_2)_{15}SH$ (**1**), referred to in the rest of this article as **C16H**] and an anthracene terminated thiol (**2**, referred to as **ANTH**), which is the ester of anthracene-2-carboxylic acid and 11-mercapto undecanol. Both the substrates have been characterised by

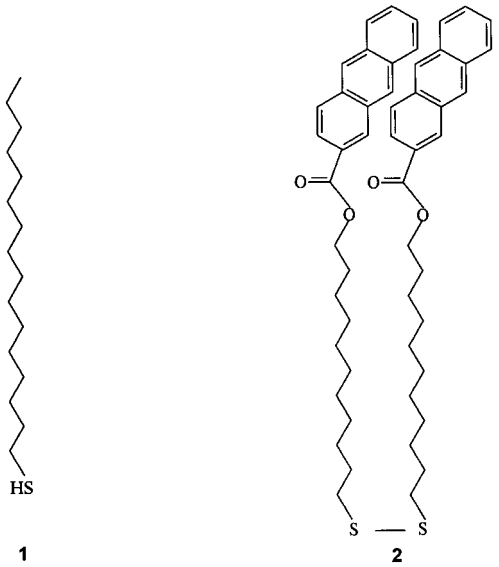

1 2

AFM investigations, which are presented here. We chose **C16H** as being a representative thiol that forms SAMs with the classical hexagonal lattice, as described later on. The polymorphs calcite and vaterite possess threefold symmetry axes (the respective space groups are *R-3c* and *P6₃/mmc*[9]), while aragonite crystallises in the orthorhombic space group *Pmcn*[10] and possesses no such threefold axis.[11] Since many thiols form hexagonal close-packed lattices,[12] aragonite templating is difficult to achieve thereon. The **ANTH** derived substrate showed greater promise for the templating of aragonite, since it forms a centred rectangular lattice when self-assembled on an Au (111) surface. The comparison gains validity from the fact that both SAMs are hydrophobic.

Another distinction of the aragonite structure is that the Ca^{2+} ions are nine-coordinate, rather than displaying the six-coordination observed in the calcite and vaterite structures. Ca^{2+} is rather small for nine-coordination. Sr^{2+} on the other hand is big enough so that the aragonite structure is the stable polymorph for $SrCO_3$. Since the crystallisation of the different polymorphs of $CaCO_3$ are complicated by competing phase amounts, rationalising the preference of one polymorph over another is not trivial. As an example, the observation of one polymorph and not another could indicate the promotion of the one as well as the inhibition of the other. We therefore felt that comparing the crystallisation of $SrCO_3$ in the aragonite/strontianite modification with the crystallisation of $CaCO_3$ in all three modifications might yield some insights into which factors are important.

The present study complements related work by Litvin et al.,[13] who have shown that the rectangular structure of the Langmuir monolayer obtained from a 5-hexadecyloxyisophthalic acid derivative can preferentially crystallise aragonite at the air–water interface through specific templating. Our use of robust, well-characterised self-assembled monolayers on solid substrates rather than of Langmuir monolayers opens up new possibilities and raises some interesting questions.

Abstract in German: *Die beiden Modifikationen von $CaCO_3$, Calcit und Vaterit, enthalten in ihrer Kristallstruktur eine dreizählige Symmetrieachse, die dritte Modifikation, Aragonit, enthält hingegen keine. Selbstorganisierte Monoschichten (SAMs) vieler einfacher Alkylthiole bilden auf Gold(111)-Oberflächen hexagonal dichteste Packungen. Diese eignen sich besonders zur templatinduzierten Kristallisation der ersten beiden $CaCO_3$-Phasen. Um speziell die Bildung des orthorhombischen Aragonits zu fördern, wurde in dieser Arbeit ein Disulfid verwendet, welches sich von einer substituierten Anthracencarbonsäure ableitet und auf Gold(111)-Oberflächen rechteckig c-zentrierte Gitter bildet. Zum Vergleich wurden Experimente auf Monoschichten aus Hexadecanthiol durchgeführt. Die Existenz von drei miteinander in Konkurrenz stehenden Phasen erschwert es, Einblicke in die Wechselwirkungen zwischen Templat und Kristall zu erhalten. Da dieses Problem beim zum Aragonit isostrukturellen System von $SrCO_3$ umgangen werden kann, wurden ebenfalls Kristallisationen des Strontianits untersucht.*

Results

AFM studies: Alkylthiols or -disulphides can be chemisorbed from solution onto clean metal surfaces (Cu, Ag, Au, etc.) whereupon they self-assemble into well-organised monolayers.[14] The two-dimensional structure of these monolayers can be influenced by various parameters including the nature and surface structure of the metal, the alkyl chain length and the ω head group. Figure 1a shows a low-magnification AFM image of the Au (111) surface covered with **C16H**. The features seen correspond to terraces on the Au (111) surface. In panel b) we show the same substrate at higher magnification, now permitting the lattice formed by a monolayer of **C16H** to be observed. The inset shows a two-dimensional Fourier transform of this image, and attests to the hexagonal structure of the SAM. The hexagonal lattice constant was determined by AFM to be 5.0 Å, which agrees well with the values of the lattice constants obtained on a series of *n*-alkanethiols.[15]

The anthracene derived disulphide **ANTH** displays a different pattern of thiol organisation. At low magnification (Figure 2a) the AFM image suggests the presence of two kinds of domains, each between 10 and 50 nm in extent. Zooming in on the two different domains it appears that there is no long-range periodicity in the darker areas, but the lighter areas display, at high magnification, a centred rectangular lattice structure (Figure 2b). The Fourier transform in the inset of Figure 2b yields the symmetry, and further analysis gives lattice parameters of 6.48 Å and 8.31 Å for the sides of

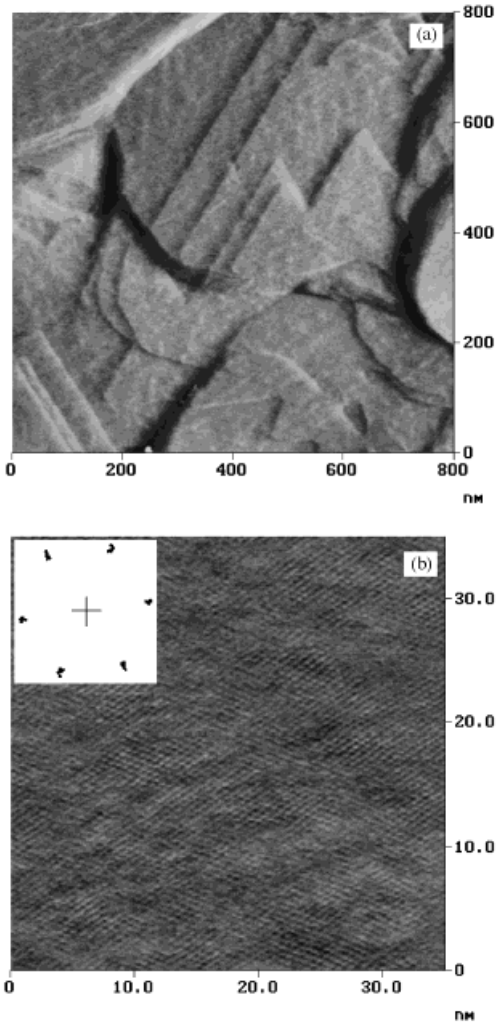

Figure 1. Atomic force micrographs of a gold surface covered with **C16H**. a) The low-magnification deflection mode image shows terraces on the gold surface. b) Higher magnification in friction mode allows the hexagonal lattice of the SAM to be seen. The inset of is a Fourier transform of the image, attesting to the hexagonal structure of the thiol monolayer.

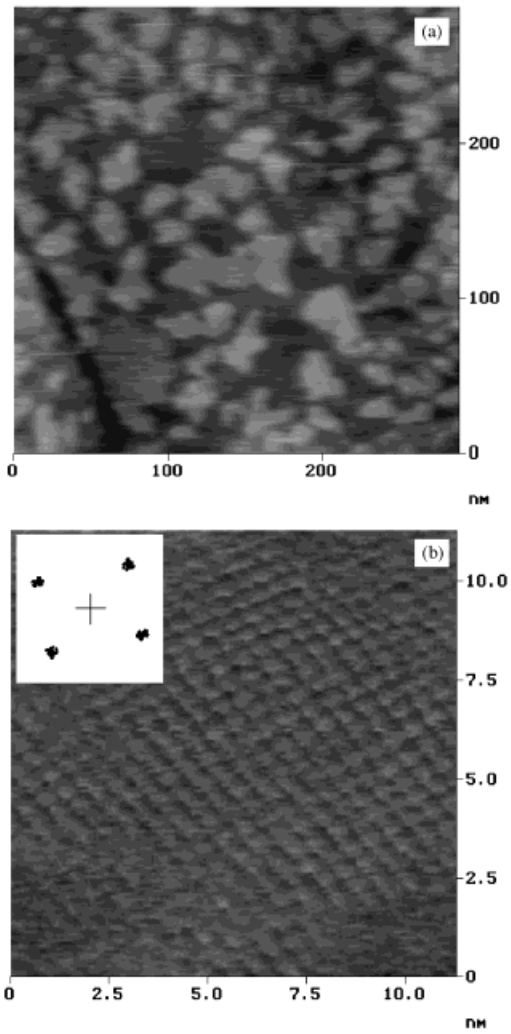

Figure 2. a) Low-magnification height-mode AFM image of an **ANTH** covered gold surface. The light and dark regions correspond to regions with and without long-range periodicity, respectively, within the thiol monolayer. b) One of the light domains of a) in higher magnification in friction mode. The lattice structure is visible and, from the Fourier transform depicted in the inset, is seen to be centered rectangular.

the centred rectangular lattice.[15] The reason for **ANTH** to organise in this manner has to do with optimal packing of the anthracene group. The profile of the anthracene head group as seen from above is approximately oval and the densest packing of ovals leads to a centred rectangular structure. Figure 3 is a sketch of the two different schemes of thiol organisation on the Au (111) surface. A comparison of the known crystal structure of anthracene[16] and of other condensed aromatics (naphthalene, tetracene etc.)[17] with the 2D lattice structure of the SAM observed here is revealing. The anthracene structure can be described as a (nearly) close packing of anthracene molecules in the *ab* plane, with the long axis of the anthracene molecules being nearly perpendicular to this plane and with every alternate molecule in the plane being oriented in a slightly different manner. In the [001] projection, the anthracene molecules display herringbone order rather than the uni-axial scheme depicted in Figure 3. However, the *a* and *b* lattice parameters of anthracene (8.56 and 6.04 Å, respectively) are very similar to those of the centred rectangular lattice determined by us. This close similarity suggests that the ellipsoids depicted in Figure 3 can therefore be considered as envelopes within which the anthracene molecule has high existence probability. The tethering of the anthracene head groups to the gold surface through long alkyl chains might also affect the nature of the packing (herringbone vs. uni-axial). Within the resolution of the present technique, these features cannot be unequivocally resolved. The different surface structures of the two SAMs presented here can be expected to influence the way they are able to template crystals.

Templated crystallisation: We have demonstrated in our earlier publications that it is possible to grow all three water-free calcium carbonate modifications, namely calcite, aragonite and vaterite, at slightly elevated temperatures.[8] Two methods have been used to collect information about phase composition and morphologies of the crystals deposited on the SAM substrates. Scanning electron (SE) microscopy provides a view of crystal habits: crystals of calcite appear

0947-6539/98/0409-1836 $ 17.50+.50/0 *Chem. Eur. J.* **1998**, *4*, No. 9

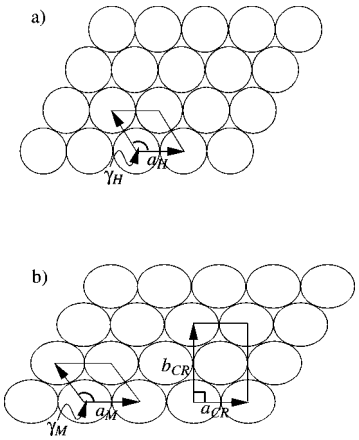

Figure 3. a) Scheme for the 2D hexagonal close packing of simple thiols such as **C16H** on Au (111) surfaces. In the case of **C16H** $a_H = 5.00(1)$ Å, and $\gamma_H = 120°$. b) Scheme for the close packing of thiols (for disulphides the shape of the thiolates is considered) that possess an oval rather than circular profile when viewed from above. The primitive monoclinic and centered rectangular lattices are outlined. For **ANTH**, $\gamma_M = 104.7°$, $a_M = 5.30(1)$ Å, $a_{CR} = 6.48(1)$ Å and $b_{CR} = 8.31(1)$ Å.

as compact rhombs, crystals of vaterite as hexagonal florets, while aragonite tends to crystallise in needles that cluster.[18] Scale factors obtained from the Rietveld refinement of the X-ray powder diffraction patterns (usually refining cell, profile and preferred orientation parameters) are then used to calculate the amounts of the individual phases.

Figure 4 illustrates the kind of X-ray powder diffraction patterns obtained from the crystals grown on the **ANTH** surface. Figure 4a shows the experimental profile (uppermost trace) and the contributions to the refined profile from the different amounts of the three polymorphs, calcite (C), vaterite (V) and aragonite (A), obtained when the crystallisation was carried out at 22 °C. The trace at the bottom is the difference in the experimental and refined profiles. Likewise, Figure 4b displays the data acquired from crystallisation experiments carried out at 45 °C on the **ANTH** surface. In this latter case the experimental data is consistent with the complete absence of vaterite and a high aragonite:calcite ratio.

The analysis of these and other X-ray diffraction profiles leads to the histograms in Figure 5, which show the phase composition of crystals collected from the two SAM surfaces as well as Au and glass references substrates at 22 °C and 45 °C. We estimate the relative spread in the data, due to fluctuations between experiments, as well as errors introduced during the analysis to be less than 10%. At 22 °C all the surfaces show nearly equal amounts of calcite and vaterite except for **ANTH**, which shows a small amount of aragonite as well. At 45 °C the possibility arises to build the high-pressure orthorhombic aragonite phase in greater quantities. On the polar glass surface calcite and aragonite are found in about equal proportions. This surface is probably representative of the thermodynamics of $CaCO_3$ formation at the two temperatures in the absence of templating effects. The organised hexagonal templates Au (111) and **C16H** clearly disfavour aragonite. On the **ANTH** surface, however, we find about 15% aragonite when the crystallisation is carried out at

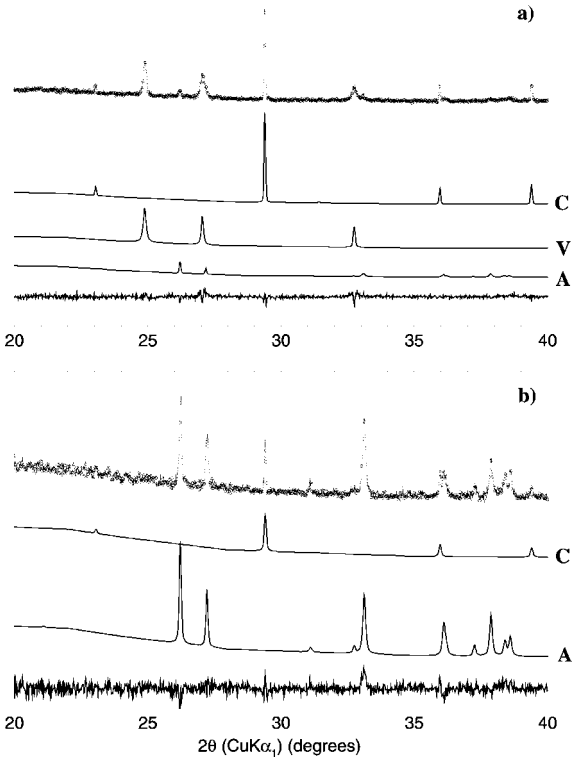

Figure 4. a) Experimental and refined powder X-ray diffraction profiles of $CaCO_3$ crystals collected from the **ANTH** surface after crystallisation at 22 °C. The experiment (top), the refined contributions due to calcite (C), vaterite (V) and aragonite (A), and the difference between the experimental and refined profiles (bottom) are shown. b) Experimental and refined powder X-ray diffraction of $CaCO_3$ crystals collected from the **ANTH** surface after crystallisation at 45 °C. Vaterite does not contribute to the refined profile.

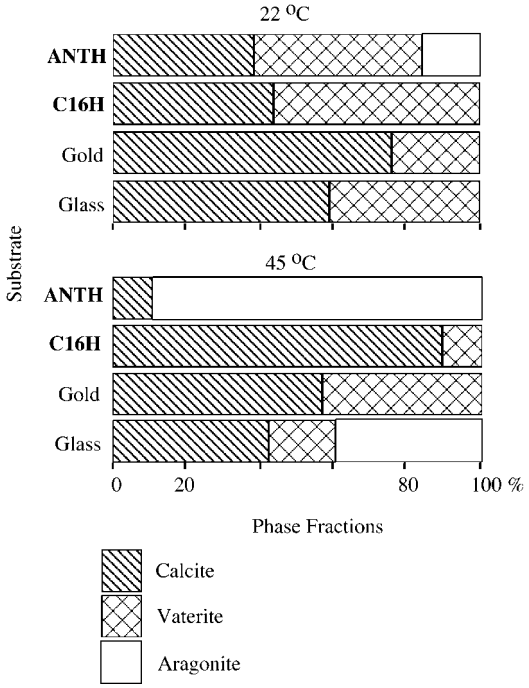

Figure 5. Histograms of the phase composition (weight fractions) of $CaCO_3$ samples collected from different surfaces after crystallisation at 22 °C and 45 °C.

  0947-6539/98/0409-1837 $ 17.50+.25/0

22 °C and nearly 90 % aragonite when the crystallisation is carried out at 45 °C.

In an attempt to understand modes of templating of the different crystal polymorphs on the ordered, well-characterised surfaces, we turn to the SE micrographs of the **C16H** and **ANTH** surfaces with the $CaCO_3$ crystals grown thereon (Figures 6 and 7). We can then proceed to draw links between the crystal habits and orientations, and the 2D structure of the template surface. Figures 6a and 6b display the **C16H** surface with the crystals of calcite (rhombs) and vaterite (florets) grown at a temperature of 22 °C. The rhombic calcite crystals are often seen as standing on a vertex. This mode of templating of the calcite crystals is explained by recognising the (001) plane of the calcite crystal as sitting flat on the SAM surface, since the dimensions of the (001) plane are in nearly perfect epitaxy with the 2D hexagonal SAM structure. In the case of vaterite, such templating is more difficult to identify. The fact that the florets stand edge-on suggests, from our knowledge of the vaterite crystal morphology, that the planes in contact with the thiol substructure could be parallel to either (100) or (110). In studying cuts of the crystal structure parallel to these planes, we are unable to identify any low index plane that might be epitaxial with the hexagonal thiol template. In panels c) and d), obtained from crystallisations on **C16H** performed at 45 °C, the clustering of the calcite rhombs on this low-polarity surface is more clearly seen though the vaterite florets are not so easily distinguished. From isolated calcite crystals, we see that the templating pattern is maintained.

Figure 7a displays all three crystal polymorphs of $CaCO_3$ formed on the **ANTH** surface at 22 °C. The calcite rhombs are now oriented in an arbitrary fashion and the vaterite florets

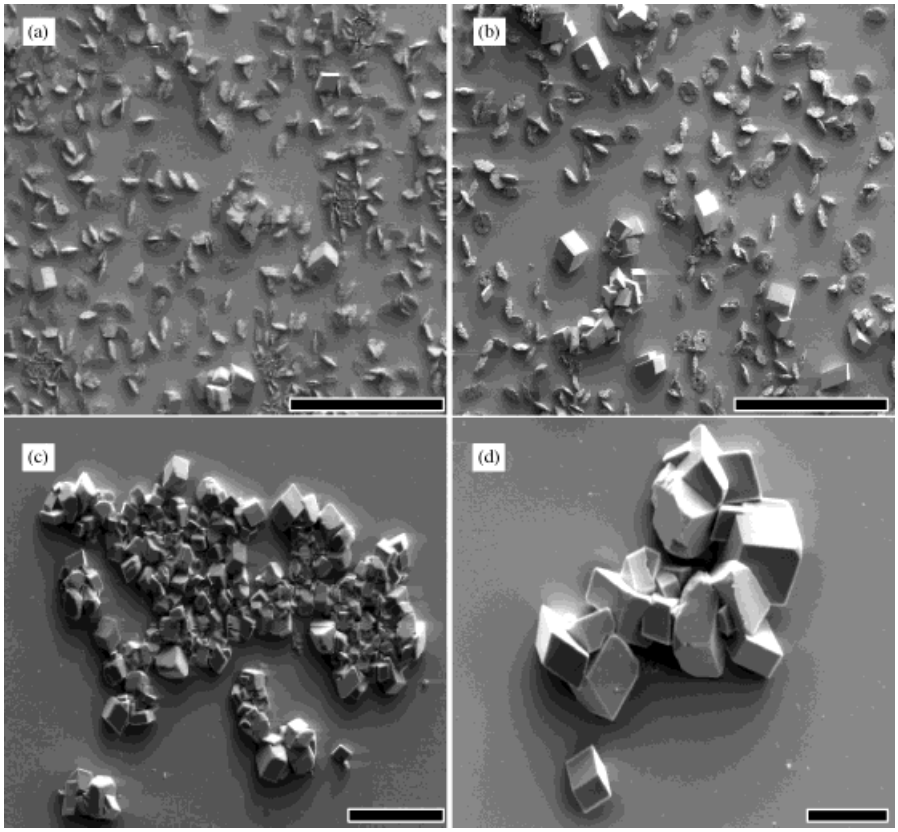

Figure 6. a) and b) SE micrographs showing crystals of calcite (rhombs) and vaterite (florets standing on edge) obtained from $CaCO_3$ crystallisation at 22 °C on **C16H** substrates. c) and d) **SE** micrographs of calcite crystals formed at 45 °C on **C16H** substrates. The scale bars are a) 200 μm, b) 200 μm, c) 50 μm and d) 20 μm.

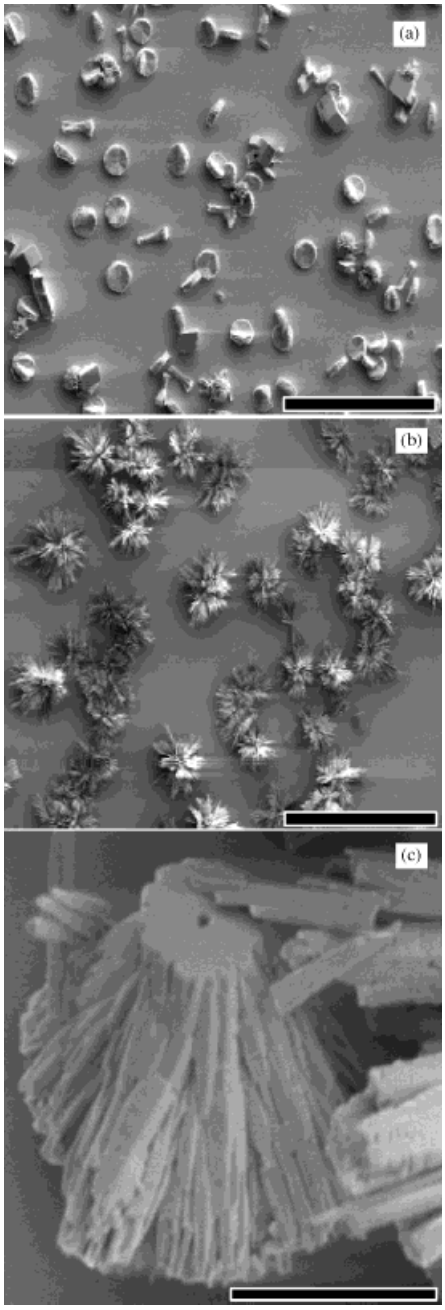

Figure 7. a) SE micrograph of $CaCO_3$ crystals formed on **ANTH** substrates at 22 °C. All three modifications, calcite rhombs, vaterite florets sitting flat and aragonite needles, are seen. b) SE micrograph of $CaCO_3$ crystals formed on the **ANTH** surface at 45 °C. The crystals are mostly aragonite, with a few calcite rhombs also being observed. c) Bundle of aragonite needles at higher magnification. The bundle is overturned and presents the flat surface on which it was nucleated. The scale bars in the panels are a) 200 μm, b) 200 μm and c) 10 μm.

0947-6539/98/0409-1838 $ 17.50+.50/0

are now seen to sit flat on their {001} crystal face. Comparing this with the micrographs in Figure 6, we evidence the effect of the different thiol structures on the crystals they template. In Figure 7a we also observe some aragonite needles clustered in the shape of a dog bone. On raising the temperature at which crystallisation is carried out to 45 °C the vaterite florets are missing (Figure 7b), consistent with the powder X-ray pattern. One observes mostly bundles of aragonite needles and a few small calcite rhombs. The calcite rhombs do not display any evidence for templating. However, the manner in which the bundles of aragonite needles resemble one another suggests that the substrate plays a specific role. In panel c) of Figure 7 we see, in high magnification, an efflorescent bundle of aragonite needles that had fortuitously turned over during the process of preparing the samples for the microscopy. The base of this bundle is extremely flat suggesting that it has been in direct contact with the SAM. The small hole in the centre is due to the growth of the bundle preventing the uniform accretion of material. The base of the bundle is about 5 μm across. We know from the AFM images that the substrates are not crystalline over such a large extent and infer that the templating cannot be homogenous throughout. What is interesting is that after growing outwards perpendicular to the surface for a few μm, the growth direction of the needles changes and they fan out. We return to this point in the discussion.

As mentioned in the introduction, the larger size of the Sr^{2+} cation ensures that the carbonate crystallises in a stable aragonite/strontianite structure. We were thus inclined to examine whether the patterns of crystallisation of $SrCO_3$ yields insight into aragonite crystallisation in the absence of competing phases. Figure 8 is the refined powder X-ray

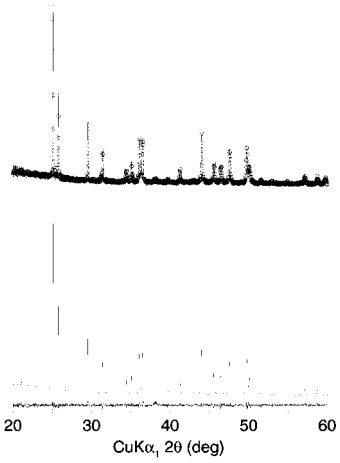

Figure 8. Experimental, refined and difference powder X-ray diffraction profiles of $SrCO_3$ in the strontianite/aragonite modification. The crystals were collected from a gold surface after crystallisation at 22 °C.

pattern of $SrCO_3$ crystallised on a clean gold substrate. There is only one crystalline phase present, namely strontianite, that has the aragonite structure, but with slightly different positional parameters and larger lattice parameters. Figures 9a and 9b compare the nature of the crystals obtained on a) clean gold and b) **ANTH** surfaces. In neither case is

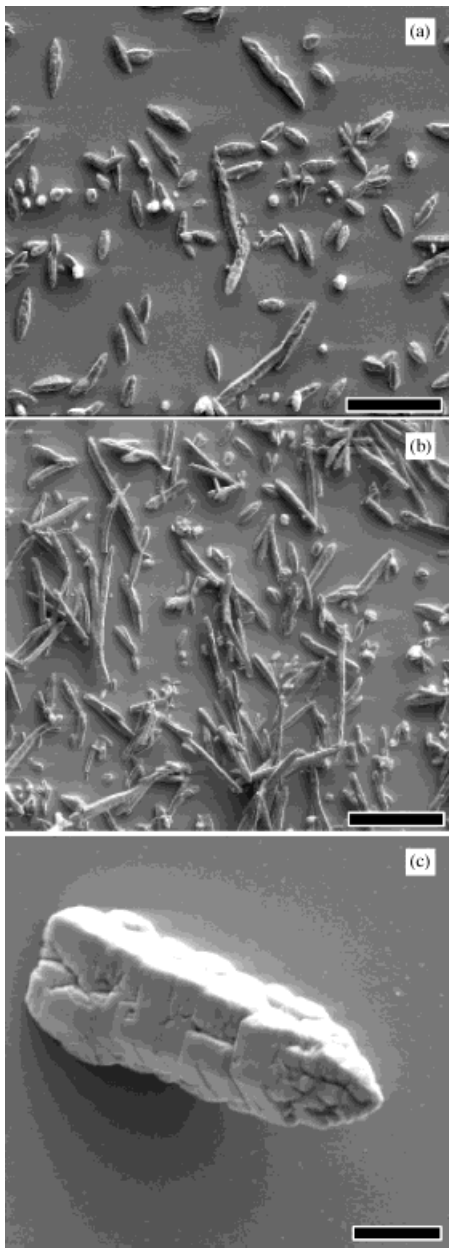

Figure 9. SE micrographs of $SrCO_3$ crystals formed a) on a gold surface and b) on the **ANTH** surface at 22 °C. c) SE micrograph of a single strontianite needle. The pseudo sixfold symmetry of the needle axis is to be noted. The scale bars are a) 50 μm, b) 50 μm and c) 5 μm.

there any evidence for a preferred growth direction and, interestingly, while the needles resemble those formed by $CaCO_3$ in the aragonite modification they do not cluster. Panel c) of Figure 9 displays one such needle in higher magnification. Of note is that the needle surface is not continuous, but fragmented and that the overall symmetry around the needle axis is sixfold.

The fact that we do not observe any obvious templating mode in the case of $SrCO_3$ on the **ANTH** surface in the present experiments is perhaps not exclusively due to the absence of a suitable mode of epitaxy, but instead could be related to the kinetics of crystallisation. The smaller solubility product of $SrCO_3$ (compared with $CaCO_3$) might result in the crystallisation taking place too rapidly for templating effects

to manifest. To further understand these aspects we attempted the crystallisation of $SrCO_3$ at 4 °C (by placing the experimental set-up in a refrigerator). At this temperature the solubility of $SrCO_3$ does not change much (from the value at 22 °C), but the $(NH_4)_2CO_3$ decomposition takes place much more slowly. Heterogeneous nucleation on the template surface therefore becomes much more important as seen from the SE micrographs in Figure 10 at a) low and b) high

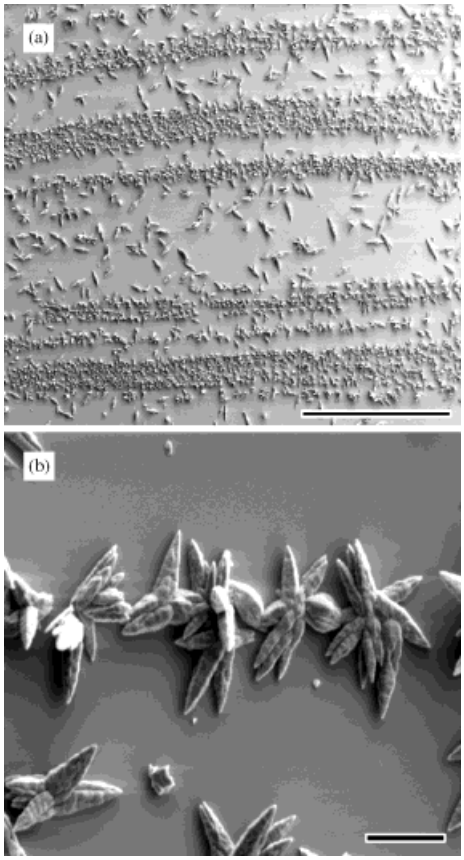

Figure 10. SE micrographs of $SrCO_3$ crystals formed on the **ANTH** surface at 4 °C at a) low magnification, showing banding or the formation of lines of crystals on the surface and b) high magnification showing the kind of bundling observed in the case of aragonite. The scale bars are a) 500 μm and b) 20 μm.

magnification. The formation of large-scale structures on the surface in the form of bands of crystals (Figure 10a) is something that we have also observed in other crystallisation experiments on thiol surfaces. The scale of the ordering (over millimetres) has nothing to do with the microscopic structure of the surface and is more likely related to Coulombic effects, which are of large-length scales. This is an aspect that needs to be investigated in detail. The florets seen in higher magnification (Figure 10b) resemble the structures formed by aragonite on this surface more closely and this suggests templating through epitaxy.

Discussion

Before attempting to correlate the 2D structure of the SAM substrates with the habits and orientations of the $CaCO_3$ crystals grown thereon, it should be noted that for the AFM studies we used mica/Au and for the templated crystallisation we used glass/Cr/Au. In the latter case we expect the planar extent of the domains of single-crystalline Au (111) to be smaller. In both cases, the size of the Au (111) domains (and therefore the SAMS) are much smaller than the $CaCO_3$ or $SrCO_3$ crystals that we examine. This is particularly true in the case of the **ANTH** substrate in which the crystalline domains extend only over 10 – 50 nanometers. The correlation between template and crystal structure is therefore justified only on assuming that the template need only act in the very early stages of crystallisation, when the nucleating crystal and the crystalline domains in the SAM substrate are similar in extent.

On the **C16H** surface, correlating the {001} face [the (001) plane] of the growing calcite crystal to the structure of the substrate is trivial and is illustrated in Figure 11a. Similar

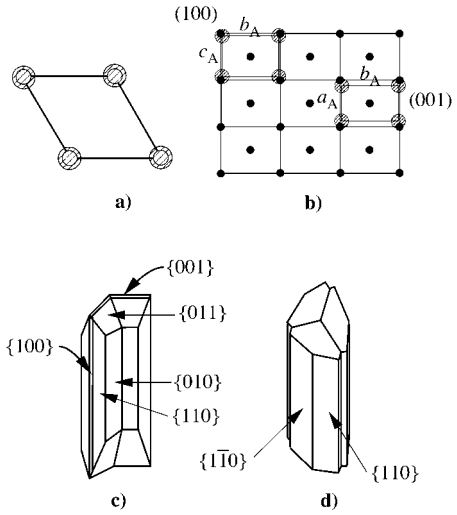

Figure 11. a) Scheme for epitaxy between the (001) plane of calcite and the underlying hexagonal (as in **C16H**) SAM substructure. The Ca atoms are depicted with hatched circles. b) Plausible modes of epitaxy between aragonite and the **ANTH** SAM lattice. The Ca atoms are depicted with hatched circles. At the upper left corner is a scheme showing the (100) plane of aragonite and the middle right section shows a scheme of the (001) plane of aragonite; both are overlayed on the centered rectangular SAM lattice. The sides of the aragonite cell are $a_A = 4.96$ Å, $b_A = 7.98$ Å and $c_A = 5.75$ Å. c) Scheme for the twinning of two typical aragonite crystals. d) Scheme for the trilling of three crystals. The crystal faces are labelled.

templating modes for vaterite do not seem as simple and indeed in the surfaces presented here we find no clear evidence for templating. Of the three polymorphs vaterite is the least stable and its formation is possibly a manifestation of Ostwald's rule of successive crystallisation, wherein atoms condense from the gas phase or precipitate from solution to yield the least stable phase first. Indeed, it is our finding that vaterite crystals redissolve over a period of time and reprecipitate as the other modifications. The case of aragonite is complicated by the way the needles tend to form bundles and the presence of twinning. In earlier contributions we have remarked on the preference of aragonite for rough or ill-formed surfaces,[7, 8] noting that it could be a result of the suppression of the other phases and/or the induction of aragonite. This lead us to attempt the growth of aragonite on a gold surface roughened by the tethering of gold colloids

0947-6539/98/0409-1840 $ 17.50+.50/0 *Chem. Eur. J.* **1998**, *4*, No. 9

through dithiols.[19] However, despite the high aragonite yields on such a surface there was no evidence for templating, with the aragonite needles found in all possible orientations. The AFM images of the **ANTH** surface shown in Figure 2 suggest that while the local symmetry in the ordered domains (and possibly also the domains with no long-range periodicity) could be centred rectangular, the alternation of ordered and disordered regions could give rise to a surface that is microscopically rough and therefore favour aragonite formation. However comparisons between the nature of the bundles of aragonite needles obtained in the present case with those obtained on the colloid-roughened surface support a picture of specific templating on the **ANTH** surface due to its 2D lattice structure.

$SrCO_3$ growth results in similar crystal morphologies when the growth is carried out on clean Au (111) or on **ANTH**, despite $SrCO_3$ being isostructural with the $CaCO_3$ modification aragonite. When the temperature is lowered to 4 °C, specific growth patterns emerge. This suggests the importance of kinetics in templated crystallisation processes.

Litvin et al.[13] suggest that on their rectangular Langmuir monolayer the preferred templating plane is (010), with the epitaxial strain being less that 10%. On the other hand, we find through a comparison of low-index planes that a plane parallel to (100) provides reasonable lattice matching with the thiol substrate as depicted in the scheme in Figure 11. This plane results in absolute lattice mismatch of 4% and 11% along the two sides. For strontianite, the same plane would result in lattice mismatch of 2% and 6%. The choice of this initial growth direction, namely [100], also allows us to reconcile the sudden fanning of the initial needles into the efflorescent bundle that is finally obtained. It would seem that secondary nucleation on the initial aragonite crystals takes place that then permits the crystal to grow along the [001] direction. This is the pseudohexagonal axis that permits the kind of threefold twinning (trilling) that is observed in higher magnification of the needles of both $CaCO_3$ and $SrCO_3$. Panel b) of Figure 11 shows plausible schemes for epitaxy between a plane parallel to the (100) and (001) planes of $CaCO_3$-aragonite and the centred rectangular thiol lattice. Considering the (001) plane the mismatch is larger, being 4% and 23% along the two sides. The chief reason for our suggesting (100) as the nucleating plane rather than (001) is not the larger mismatch of the latter, but the observation that the needles fan out after growing a few micrometres. Panel c) of Figure 11 displays the labelling of the crystal faces of a typical twin of aragonite and panel d) shows a trilling, as presented in the literature.[20] We propose that each needle of aragonite or strontianite is such a trilling and the bundling is caused due to the sudden change in the growth direction from that of the original template, plausibly from [100] to the [001] needle direction. In the absence of realistic computer simulations of the nucleation and growth of $CaCO_3$ on the SAM substrates, we can only speculate on the nature of the initial interaction. Considering the low polarity of the substrates used here, we can expect that carbonate ions would be in close contact with the organic substrates. In the case of aragonite nucleating on the (100) plane on the ANTH substrate, it would appear that the triangular carbonate groups nucleate with the plane of this group perpendicular to the plane of the substrate and that one of the oxygen atoms is in closest contact to the substrate.

Experimental Section

Details of the AFM measurements on SAMs of a number of different thiols can be found in refs. [15, 21] and of the templated crystallisation experiments in ref. [8]. Hexadecanethiol (abbreviated **C16H**, synthesis grade) was purchased from Merck and $SrCl_2 \cdot 6H_2O$ (PA) from Fluka. The synthesis of the disulphide $[(C_{14}H_9)COO(CH_2)_{11}S]_2$ is described in ref. [22]. For the AFM measurements Au (111) substrates were prepared by evaporating 100 nm Au onto freshly cleaved mica in vacuum of around 10^{-4} Pa at an evaporation rate of 0.2 nm s^{-1} employing a Baltec MED 020 coating system. After coating, the substrates were heated rapidly to 400 °C in a purpose-built chamber and then quenched in a methanol bath to room temperature. SAMs were prepared by placing the gold-coated substrates for 12 to 18 hours in a 10^{-4}–10^{-3} M solution of the corresponding thiol or disulphide in ethanol or dichloromethane, followed by removal and extensive rinsing. The measurements were done in a fluid cell with a Nanoscope IIIa. The samples were imaged under ethanol in contact mode with silicon nitride cantilevers of 100 μm length with sharpened tips (spring constant 0.09 N m^{-1}, Olympus). Details of image analysis are described elsewhere.[21]

The crystallisation of calcium (strontium) carbonate was carried out on glass-slide substrates, which were coated with 2 nm Cr, 50 nm Au and a thiol SAM, over a 48 h period by holding the slides with the active surface down in temperature- and pH-controlled solutions of $CaCl_2$ or $SrCl_2$. Solid $(NH_4)_2CO_3$ was used as a CO_2 source for the precipitation. The powder XRD measurements were performed in the $\theta/2\theta$ transmission geometry with a Siemens D5000 powder diffractometer with Ge(111) monochromatized $Cu_{K\alpha}$ radiation (1.54056 Å). Crystals were scraped from the surface and mounted on Scotch™ tape. Data were collected from 20° to 60° 2θ, with a step size of 0.02° and a count time of 25 seconds per step. Because of the very small yields, it was necessary to collect samples from three to four substrates for each experiment. The powder diffraction patterns were subject to Rietveld refinement[23] by means of the XND computer program.[24] SE micrographs were acquired on a Zeiss DSM 962 at acceleration tensions of 5–15 kV. The substrates on which the crystallisation was carried out were cut in small pieces, fastened with conducting glue on aluminium sample holders and sputtered with gold before inserting into the SE microscope.

Acknowledgments: We thank Professor Wolfgang Knoll (Max-Planck-Institut für Polymerforschung) for help and encouragement, and the Degussa AG for a gift of gold. G.N. is supported by the Ernst Rudolf Schloeßmann-Stiftung.

Received: February 6, 1998 [F987]

[1] a) A. Lowenstam, S. Weiner, *On Biomineralization*, Oxford University Press, New York, **1989**; b) *Biomineralization*, (Eds.: S. Mann, J. Webb, R. J. P. Williams) VCH, Weinheim, **1989**.

[2] a) S. Weiner, L. Addadi, *Angew. Chem.* **1992**, *104*, 159; *Angew. Chem. Int. Ed. Engl.* **1992**, *31*, 153; b) S. Weiner, S. Albeck, L. Addadi, *Chem. Eur. J.* **1996**, *2*, 278.

[3] a) S. Rajam, B. R. Heywood, J. B. A. Walker, S. Mann, R. J. Davey, J. D. Birchall , *J. Chem. Soc. Faraday Trans.* **1991**, *87*, 727; b) B. R. Heywood, S. Mann, *Chem. Mater.* **1994**, *6*, 311.

[4] D. D. Archibald, S. B. Quadri, B. P. Gaber, *Langmuir* **1996**, *12*, 538.

[5] a) B. J. Brisdon, B. R. Heywood, A. G. W. Hodson, S. Mann, K. K. W. Wong, *J. Mater. Chem.* **1994**, *4*, 1387; b) B. J. Brisdon, B. R. Heywood, A. G. W. Hodson, S. Mann, K. K. W. Wong, *Adv. Mater.* **1993**, *5*, 49; c) J. M. Marentette, J. Norwig, E. Stöckelmann, W. H. Meyer, G. Wegner, *Adv. Mater.* **1997**, *9*, 647; d) G. Falini, M. Gazzoni, A. Ripamonti, *Adv. Mater.* **1994**, *6*, 46.

[6] a) D. Walsh, S. Mann, *Adv. Mater.* **1997**, *9*, 658; b) S. Mann, S. L. Burkett, S. A. Davis, C. E. Fowler, N. H. Mendelson, S. D. Sims, D.

Walsh, N. T. Whilton, *Chem. Mater.* **1997**, *9*, 2300; c) T. Hirai, S. Hariguchi, I. Komasawa, *Langmuir* **1997**, *13*, 6650.
[7] J. Küther, W. Tremel, *Chem. Commun*. **1997**, 2029.
[8] J. Küther, R. Seshadri, W. Knoll, W. Tremel, *J. Mater. Chem.* **1998**, *8*, 641.
[9] a) R. Wartchow, *Zeit. Kristallogr.* **1989**, *186*, 300; b) S. R. Kamhi, *Acta Crystallogr*. **1963**, *16*, 770.
[10] We retain this nonstandard setting of the *Pnma* space group in keeping with the original description of Bragg; W. Bragg, *Proc. Roy. Soc. A*. **1924**, *105*, 16; see also J. P. R. de Villiers, *Am. Mineral.* **1971**, *56*, 758.
[11] Megaw has pointed out that when projected down [001], the structure looks nearly pseudohexagonal and this is an important physical characteristic resulting in crystals that usually displaying considerable trilling around this axis, thus giving rise to six-sided needles: H. Megaw, *Crystal Structures*, *A Working Approach*, W. B. Saunders, Philadelphia, **1973**.
[12] a) A. Ulman, *Chem. Rev*. **1996**, *96*, 1533; b) A. Ulman, *MRS Bulletin* **1995**, 46.
[13] A. L. Litvin, S. Valiyaveettil, D. L. Kaplan, S. Mann, *Adv. Mater*. **1997**, *9*, 124.
[14] a) P. E. Laibinis, G. M. Whitesides, D. L. Allara, Y. T. Tao, A. N. Parikh, R. G. Nuzzo, *J. Am. Chem. Soc.* **1991**, *113*, 7152; b) P. E. Laibinis, G. M. Whitesides, *J. Am. Chem. Soc*. **1992**, *114*, 1990; c) L. Strong, G. M. Whitesides, *Langmuir* **1988**, *4*, 546; d) C. E. D. Chidsey, Y. G. Liu, P. Rowntree, G. J. Scoles, *J. Chem. Phys.* **1989**, *91*, 4421; e) C. A. Alves, E. L. Smith, M. D. Porter, *J. Am. Chem. Soc*. **1992**, *114*, 1222; e) E. Delamarche, B. Michel, C. Gerber, D. Anselmetti, H. J. Güntherodt, H. Wolf, H. Ringsdorf, *Langmuir* **1994**, *10*, 2869.
[15] G. Nelles, H. Schönherr, M. Jaschke, H. Wolf, M. Schaub, J. Küther, E. Bamberg, H. Ringsdorf, H.-J. Butt, *Langmuir* **1998**, *14*, 808.
[16] a) A. M. Mathieson, J. M. Robertson, V. C. Sinclair, *Acta Crystallogr.* **1950**, *3*, 245; b) V. C. Sinclair, J. M. Robertson, A. M. Mathieson, *Acta Crystallogr*. **1950**, *3*, 251.
[17] A. I. Kitaigorodsky, *Molecular Crystals and Molecules*, Academic Press, New York, **1973**.
[18] Y. Ota, S. Inui, T. Iwashita, T. Kasuga, Y. Abe, *J. Am. Ceram. Soc*. **1995**, *78*, 1983.
[19] J. Küther, R. Seshadri, G. Nelles, H.-J. Butt, W. Knoll, W. Tremel, *Adv. Mater.* **1998**, *10*, 401.
[20] H. L. Monaco, D. Viterbo, F. Scordari, G. Gilli, G. Zanotti, M. Catti, *Fundamentals of Crystallography* (Ed.: C. Giacovazzo), Oxford University Press, Oxford, **1992**.
[21] M. Jaschke, H. Schönherr, H. Wolf, H.-J. Butt, E. Bamberg, M. K. Besocke, H. Ringsdorf, *J. Phys. Chem*. **1996**, *100*, 2290.
[22] M. Schaub, M. S. Wrighton, (unpublished results).
[23] H. M. Rietveld, *J. Appl. Crystallogr*. **1969**, *2*, 65.
[24] J. F. Berar, Computer Code XND version 1.16, European Synchrotron Radiation Facility, Grenoble, France, **1997**.

0947-6539/98/0409-1842 $ 17.50+.50/0 *Chem. Eur. J.* **1998**, *4*, No. 9